Electrical conductivity of anhydrous and hydrous gabbroic melt under high temperature and high pressure: Implications for the high conductivity anomalies in the region of mid–ocean ridge

Mengqi Wang[1,2], Lidong Dai[1*], Haiying Hu[1*], Ziming Hu[1,2], Chenxin Jing[1,2], Chuanyu Yin[1,2], Song Luo[1,2] and Jinhua Lai[1,2]

[1]*Key Laboratory of High-temperature and High-pressure Study of the Earth's Interior, Institute of Geochemistry, Chinese Academy of Sciences, Guiyang, China*

[2]*University of Chinese Academy of Sciences, Beijing, China*

To be submitted to ***Solid Earth***

February 26th, 2023

*Authors to whom correspondence should be addressed: dailidong@vip.gyig.ac.cn and huhaiying@vip.gyig.ac.cn

Abstract

The electrical conductivity of gabbroic melt with four different water contents (i.e. 0, 2.59 wt%, 5.92 wt% and 8.32 wt%) was measured at temperatures of 873–1373 K and pressures of 1.0–3.0 GPa using YJ–3000t multi–anvil high−pressure apparatus and Solartron–1260 impedance spectroscopy analyzer. At a fixed water content of 2.59 wt%, the electrical conductivity of the sample slightly decreased with increasing pressure at the temperature range of 873–1373 K, and its corresponding activation energy and activation volume were determined as 0.87 ± 0.04 eV and –1.98 ± 0.02 cm^3 $mole^{-1}$, respectively. Under the certain conditions of 873–1373 K and 1.0 GPa, the electrical conductivity of the gabbroic melts tends to gradually increase as the rise of water content from 0 to 8.32 wt%, and the activation enthalpy decreases from 0.93 eV to 0.63 eV, accordingly. Furthermore, the functional relation models for the electrical conductivity of gabbroic melts with the variations of temperature, pressure and water content were constructed at high–temperature and high–pressure conditions, respectively. In addition, the dependence relation of the electrical conductivity of melts with the degree of depolymerization was explored under conditions of four different water contents, 1373 K and 1.0 GPa, and three previously available reported results on those of representative calc–alkaline igneous rock melts (i.e. dacitic melt, basaltic melt and andesitic melt) were detailedly compared. In comprehensive combination with our presently acquired electrical conductivity data of gabbroic melt with four different water contents and the available data of polycrystalline olivine, the electrical conductivity of gabbroic melt–olivine system on

the variation of volume percentage of anhydrous and hydrous melts was successfully constructed by virtue of the typical Hashin–Shtrikman upper bound model. In light of the electrical conductivity of gabbroic melt–olivine system with the previous MT results, we find that the anhydrous and hydrous gabbroic melts can be employed to reasonably interpret the high conductivity anomalies in the Mohns ridge of the Arctic Ocean.

Keywords: electrical conductivity, gabbroic melt, degree of depolymerization, high conductivity anomalies, Mohns ridge

1 Introduction

The hydrous melt for various rocks and minerals widely exists at active plate tectonic boundaries such as mid–ocean ridge, subduction zone, orogenic belt, etc. (Shen and Forsyth, 1995; White et al., 2001; Wallace, 2005; Wu et al., 2018; Sim et al., 2020; Förster and Selway, 2021; Li et al., 2022; Turner and Langmuir, 2022). For the typical Mohns ridge in the Arctic Ocean, there existed a large amount of high conductivity anomaly phenomena with its correspondent magnitude of 0.08–0.32 S m^{-1} for the gabbro–rich regions have been revealed on the basis of previous magnetotelluric (MT) controlled source electromagnetic (CSEM) results (Johansen et al., 2019).

Previously available researches have indicated that gabbroic and basaltic melts contain a large amount of water, and the water content for the certain type of melt may be discrepant within the different depth ranges of the oceanic crust (Dixon et al., 1995; Almeev et al., 2008; Shaw et al., 2010; Leuthold et al., 2018). Meanwhile, water content is also considered as a crucial ingredient to possibly affect the electrical conductivity of melt, and there are a large number of previously available reported results for the variation of water content on the electrical conductivity of some representative calc–alkaline igneous rock melts at high temperature and high pressure in the recently several years (Ni et al., 2011; Laumonier et al., 2015; Guo et al., 2017; Chen et al., 2018). For example, Ni et al. (2011) measured the electrical conductivity of hydrous basaltic melt within water content range of 0–6.3 wt% at conditions of 1473–1923 K and 2.0 GPa, and they found that the electrical conductivity of basaltic

63 melt with a fixed water content of 6.3 wt% was of the rough 1.0 order of magnitude
64 higher than that of the anhydrous sample. The electrical conductivity of dacitic melt
65 within the water content range of 0–12 wt% was systematically investigated by
66 Laumonier et al. (2015) within temperature range of 673–1623 K and pressures of
67 0.3–3.0 GPa. As pointed out by Laumonier et al. (2015), the high conductivity
68 anomalies in the Uturuncu Volcano could be explained by the presence of hydrous
69 dacitic melt. By virtue of a piston cylinder high–pressure apparatus and sweeping–
70 frequency impedance spectroscopy, Guo et al. (2017) obtained the electrical
71 conductivity data of andesitic melt within the water content range of 0.01–5.90 wt% at
72 conditions of 1164–1573 K and 0.5–1.0 GPa. Their experimental results indicated that
73 the presence of less than 20 vol% of hydrous andesitic melt within the water content
74 range of 6–9 wt% can be used to interpret the high conductivity anomalies beneath the
75 surface of the Uturuncu Volcano. Electrical conductivity measurements of the
76 hydrous leucogranitic melt by Chen et al. (2018) at conditions of 739–1680 K and
77 0.36–2.52 GPa were systematically carried out within the water content range of
78 2.73–11.97 wt%. In comprehensive combination with previous magnetotelluric data
79 in the northwest Himalaya, they considered that water–rich leucogranitic melts with a
80 volume percentage range of 4–16 vol% can be applied to reasonably explain the high
81 conductivity anomalies in these regions.

82 For the natural gabbroic rock, some previously available electrical conductivity
83 results were obtained using the piston–cylinder and multi–anvil high–pressure
84 apparatus at high temperature and high pressure. Sato and Ida (1984) measured the

electrical conductivity of the olivine–gabbro containing gabbroic melt at the temperature range from 1123 K to 1473 K and atmospheric pressure, and the effects of ionic diffusion of charge carriers (i.e. sodium, iron, magnesium and/or calcium ions) and geometric structure of melt on the electrical conductivity of olivine–gabbro samples were detailedly explored. The measurements of electrical conductivity for natural gabbro were carried out at conditions of 1023–1423 K and room pressure by Schilling et al. (1997), and they proposed that the electrical conductivity of samples can be enhanced by the increasing volume percentage of gabbroic melt. As for the natural Oman gabbro, the electrical conductivity of gabbroic melt with the volume percentage proportion of 34 % was ~1.0–2.0 orders of magnitude higher than that of melt–free sample within the temperature range from 1073 K to 1523 K and pressures of 0.3–1.0 GPa (Maumus et al., 2005). However, the influence of water content on the electrical conductivity of gabbroic melt at high temperature and high pressure was not investigated in detail. Consequently, it is crucial to make a systematic investigation on the electrical conductivity of gabbroic melt with different water contents at high–temperature and high–pressure conditions.

In the present studies, a series of electrical conductivity on the gabbroic melts were systematically performed under conditions of 873–1373 K, 1.0–3.0 GPa and the variation of water content range from 0 to 8.32 wt%. The effects of temperature, pressure and water content on the electrical conductivity of gabbroic melt are deeply explored, and the functional relation models have been successfully established at high–temperature and high–pressure conditions. In conjunction with the degree of

depolymerization, the electrical conductivity of gabbroic melt with different water contents is compared with that of three representative calc–alkaline igneous rock melts (i.e. dacitic melt, andesitic melt and basaltic melt). Based on the calculated electrical conductivity of gabbroic melt–olivine system, its potential geophysical implication was detailedly discussed in the Mohns ridge of the Arctic Ocean.

2 Experimental procedures

2.1 Sample Preparation

The natural gabbroic rock used in this study was collected from the ophiolite suite in the region of Ganzi Tibetan autonomous prefecture, Sichuan province, China. By virtue of the high–temperature quenched melt for the natural rock powder, the anhydrous and hydrous gabbroic melts are successfully obtained. Firstly, the fresh natural gabbro was finely crushed and ground into the sample powder with the grain size of less than 50 μm in an agate mortar. Then, the sample powder was kept in the furnace at 473 K to remove the absorbed water. To obtain the homogeneously initial materials for the subsequent electrical conductivity measurement, the powder of gabbroic rock was melted at the temperature of 1473 K for 1.5 hours and rapidly quenched in a high–temperature muffle furnace. Further, gabbroic melt was crushed and ground again into powder with a grain size less than 50 μm and stored in a vacuum dry furnace at 373 K. To synthesize the hydrous gabbroic melt, the desired amount of deionized water was added to the powder, and subsequently, the sample encapsulated in a gold tube using the Lampert–Puk precise welding device. After that, the starting hydrous gabbroic melts with different water contents were synthesized at

conditions of 1373 K and 1.0–3.0 GPa for 12 hours in the YJ–3000t multi−anvil high−pressure apparatus, and all of these obtained samples are homogeneous without any available crystals or bubbles. Detailed hot–pressed sintering assemblage was similar to that previously described by Hu et al. (2022a). Lastly, all of the gabbroic melts were polished into cylinders with diameters of ~4.0–5.0 mm and heights of ~4.0–6.0 mm, and kept in muffle furnace at 423 K for 10 hours to eliminate the absorbed water for subsequent electrical conductivity measurements. The chemical compositions of anhydrous and hydrous gabbroic melts were analyzed by virtue of the electronic probe microscopy analysis (EPMA) at the State Key Laboratory of Ore Deposit Geochemistry, Institute of Geochemistry, Chinese Academy of Sciences, Guiyang, China, as shown in Table 1.

2.2 High–pressure cell and impedance measurements

High–pressure complex impedance measurements for gabbroic melt were performed by using Solartron–1260 impedance spectroscopy analyzer in the YJ–3000t multi–anvil high–pressure apparatus. The cross–section diagram of sample assembly for electrical conductivity measurements was shown in Fig. 1. Before high–pressure cell was assembled, the cubic pressure medium of pyrophyllite with dimension of 32.5×32.5×32.5 mm^3 and insulation sleeves were baked at 1073 K in a muffle furnace for 5 hours to remove the absorbed water. The sample was placed at the middle of the alumina and magnesia insulation sleeves, and sandwiched with two symmetric nickel electrodes. The electrode was connected with a $Ni_{97}Al_3$ wire to a Solartron–1260 impedance spectroscopy analyzer. To shield against external electromagnetism and

spurious signal interference, the nickel foil with a thickness of 0.025 mm was installed between the alumina and magnesia sleeves, and linked to the Earth line. Three–layer stainless steel sheets with a total thickness of 0.5 mm were adopted as the heater, which were installed between the cubic pressure medium of pyrophyllite and alumina sleeve. After that, the sample assembly was stored in the vacuum dry furnace at 423 K for at least 12 hours before the electrical conductivity measurements.

During the experiment, the pressure was slowly raised with a rate of 1.0 GPa h^{-1} until it reached the desired value, and then the temperature was gradually increased with a speed of 5.0 K min^{-1}. Under predesignated high–temperature and high–pressure condition, impedance spectra of samples were collected in the frequency range of 10^0–10^6 Hz and the applied signal voltage of 1.0 V. To obtain reproducible data, impedance spectra of samples were measured at least two continuously heating–cooling cycles under conditions of 873–1373 K and 1.0–3.0 GPa. The uncertainties of temperature and pressure were less than 5.0 K and 0.1 GPa, respectively. The detailed experimental principles and measurement procedures were described by Dai et al. (2008) and Hu et al. (2022b).

2.3 Determination of the water content

The water content of gabbroic melt before and after the electrical conductivity measurements was performed by virtue of the Vertex−70V and Hyperion−1000 vacuum Fourier transform infrared (FT–IR) spectroscopy analyzer. The samples were double–polished up to a thickness of ~50 μm. At least five spectra were conducted on the different regions of transparent sample surfaces and made an average value in

order to avoid the heterogeneity effect of water distribution. A detailed experimental method and procedure for the FT–IR measurement was detailedly presented by Hong et al. (2022) and Hu et al. (2022b). For the hydrous gabbroic melts, the signal of the fundamental stretching H_2O vibrational spectroscopy at the peak position of ~3530 cm^{-1} revealed to be oversaturated, which was similar to the previously obtained results on hydrous dacitic melts reported by Laumonier et al. (2015). Two obviously characteristic peaks were appeared at two correspondent wavenumbers of ~4500 cm^{-1} and ~5200 cm^{-1}, which were representing the hydroxyl band and molecular water band of gabbroic melts, respectively (Stolper, 1982; Dixon et al., 1995). Hence, the peak area for the hydroxyl band and molecular water band was integrated to determine the water content of sample. The typical FT–IR spectra of gabbroic melt within the wavenumbers range of 2500–5800 cm^{-1} are shown in Fig. 2. The water content of gabbroic melt (C_{melt}) can be worked out by Beer–Lambert law,

$$C = \omega A/\varepsilon\rho d \quad (1)$$

$$C_{melt} = C_{OH}+C_{H_2O} \quad (2)$$

In here, the signal of ω stands for the molar mass of H_2O (18.02 g $mole^{-1}$), A stands for the integrated area of absorption spectra (cm^{-2}), ρ stands for the density (g cm^{-3}), d stands for the thickness of thin section (cm), and ε stands for the integral molar absorption coefficient (L $mole^{-1}\cdot cm^{-2}$). As presented the calculated melt density method by Luhr (2001), our density of gabbroic melt is determined as 2.764×10^3 g L^{-1}. Molar absorption coefficients of ε_{OH} and ε_{H_2O} were adopted from Dixon et al. (1995). According to the Eqs. 1 and 2, the water contents for three obtained hydrous

gabbroic melts were calculated as 2.59 wt%, 5.92 wt% and 8.32 wt%, respectively. As displayed in Table 2, there is no significant loss of water for hydrous gabbroic melt during the electrical conductivity experiment. At the same time, the corresponding error bars of each water contents for the initial and recovered gabbroic melts are detailedly included in Table 2.

3 RESULTS

In the present experiments, the electrical conductivity of gabbroic melt with four different water contents (i.e. 0, 2.59 wt%, 5.92 wt% and 8.32 wt%) was measured at temperature range of 873–1373 K and pressures of 1.0–3.0 GPa. The representative complex impedance spectra of gabbroic melt with the 2.59 wt% water at conditions of 873–1373 K and 2.0 GPa were shown in Fig. 3. According to the theory of *AC* complex impedance spectra, the impedance spectra of gabbroic melts within the high-frequency range from ~10^2–10^3 Hz to 10^6 Hz can be interpreted as the bulk conduction mechanism (i.e. grain interior), and whereas, the impedance spectra of sample within the low-frequency range from 10^0 Hz to ~10^2–10^3 Hz represent the grain boundary conduction mechanism or the polarization process at sample–electrode interface (Tyburczy and Roberts (1990), Dai et al. (2008, 2012, 2013, 2014, 2016); Dai and Karato (2009a, b, c, 2020)). And thus, a series connection of R_S–CPE_S (R_S and CPE_S represent the resistance and constant–phase element of the gabbroic melt, respectively) and R_E–CPE_E (R_E and CPE_E represent the interface resistance and constant–phase element for electrode effect, respectively) were employed as the equivalent circuit within a relatively lower temperature range of 873–1123 K. As far

as the higher temperature ranges of 1173–1373 K, the equivalent circuit was consisted of the series connection of one resistance and one parallel resistance with the constant phase element (CPE). The electrical conductivity of sample can be calculated,

$$\sigma = L/SR \tag{3}$$

In here, L, S and R stand for the length of sample (m), the cross–section area of electrode (m^2) and the electrical resistance of sample (Ω), respectively. And the electrical conductivity of gabbroic melt and temperatures conformed to the Arrhenius relation,

$$\sigma = \sigma_0 \exp(-\Delta H/kT) \tag{4}$$

In here, σ_0 stands for the pre–exponential factor (S m^{-1}), k stands for the Boltzmann constant (eV K^{-1}), and T stands for the absolute temperature (K), respectively. All of these fitted parameters for the electrical conductivity of anhydrous and hydrous gabbroic melt under conditions of 873–1373 K and 1.0–3.0 GPa were listed in Table 2.

For the gabbroic melt with a fixed water content of 2.59 wt%, the electrical conductivity results for two continuously heating–cooling cycles at 873–1373 K and 3.0 GPa were shown in Fig. 4. In the first heating cycle within the temperature range of 923–1073 K, the electrical conductivity of sample was slightly deviated with those of subsequent results in the first cooling and second heating–cooling cycles. Whereas, the deviation degree became more and more small and finally overlapped at much higher temperature range of 1123–1373 K. As a whole, the electrical conductivity of sample was almost reproducible in the first cooling and second heating–cooling cycles.

239 And therefore, the electrical conductivity results were acquired by virtue of fitting
240 experimental data during the process of the first cooling and second heating–cooling
241 cycles.

242 **4 Discussions**

243 **4.1 Influence of pressure on electrical conductivity**

244 To identify the effect of pressure on the electrical conductivity of sample, the
245 electrical conductivity of hydrous gabbroic melt was acquired under condition of 873–
246 1373 K, 1.0–3.0 GPa and a fixed water content of 2.59 wt%. As illustrated in Fig. 5,
247 the electrical conductivity of sample and temperature conformed to the Arrhenius
248 relation at a certain water content and pressure condition. In the present studies, a
249 slightly negative dependence relation for the electrical conductivity of hydrous
250 gabbroic melt with a fixed water content of 2.59 wt% on the pressure was observed.
251 The electrical conductivity of sample slightly decreases by around 1.6 times at as
252 pressure enhances from 1.0 GPa to 3.0 GPa at temperature range of 873–1373 K.
253 Accordingly, the pre–exponential factor reduces from 3.02×10^3 S m^{-1} to 6.17×10^2 S
254 m^{-1}, and the activation enthalpy value decreases from 0.85 eV to 0.81 eV,
255 respectively.

256 Furthermore, the influence of pressure on the electrical conductivity of gabbroic
257 melt can be depicted as,

258 $$\sigma = A_0(1-BP)\cdot\exp[-\frac{\Delta U+P\Delta V}{kT}] \quad (5)$$

259 In here, the pre–exponential factor (σ_0) and activation enthalpy (ΔH) of pressure
260 dependence can be illustrated as the relations of $\sigma_0 = A_0(1-BP)$ and $\Delta H = \Delta U+P\Delta V$.

All of the listed parameters including ΔU, ΔV, and P stand for the activation energy (eV), the activation volume (cm^3 $mole^{-1}$) and pressure (GPa), and as well as B is representing a constant, respectively. Furthermore, the electrical conductivity of gabbroic melt along with the variations of temperature, pressure and water content is fitted accordingly and the detailed fitting results are displayed in Table 3. The logarithmic electrical conductivity of gabbroic melt with a fixed water content of 2.59 wt% and the inverse temperature follows a good linear relation, which reveals only one main conduction mechanism operating the electrical transport within our experimental temperature and pressure ranges. By virtue of the available pressure–dependent electrical conductivity, we also can extrapolate the relationship between the electrical conductivity of gabbroic melt with a fixed water content of 2.59 wt% and temperature at atmospheric pressure. And then the pre–exponential factor and activation enthalpy at room pressure are calculated as 5177 S m^{-1} and 0.87 eV, respectively. According to Eq. 5 and Table 3, the activation energy and activation volume of gabbroic melt with a fixed water content of 2.59 wt% can be determined as 0.87 ± 0.04 eV and -1.98 ± 0.52 cm^3 $mole^{-1}$.

4.2 Influence of water content on electrical conductivity

For a fixed pressure of 1.0 GPa, the influence of water content on the electrical conductivity of gabbroic melt at temperature range of 873–1373 K is detailedly shown in Fig. 6. The electrical conductivity of gabbroic melt with four different water contents gradually increases with the rise of temperature. For each correspondent water content (i.e. 0, 2.59 wt%, 5.92 wt% and 8.32 wt%), the logarithm of electrical

conductivity of the sample and reciprocal temperature follows a good linear relation. On the other hand, when water content of gabbroic melt enhances from 0 to 8.32 wt%, the electrical conductivity of gabbroic melts tends to visibly increase, and whereas the activation enthalpy gradually reduces from 0.93 eV to 0.63 eV, accordingly. In short, our presently acquired electrical conductivity results show a substantial enhancement of water on the electrical conductivity of gabbroic melt, which are also observed among the electrical conductivity of other representative calc–alkaline igneous rock melts in the recent years (Ni et al., 2011; Laumonier et al., 2015; Guo et al., 2017; Chen et al., 2018).

The electrical conductivity of hydrous gabbroic melt can be expressed in terms of the charge species concentration dependence of the pre–exponential factor (A), which behaves in an Arrhenius relation,

$$\sigma = (A_1 + A_2 \cdot C_w^r) \cdot \exp\left(\frac{-\Delta H_0 - \alpha C_w^\beta}{RT}\right) \quad (6)$$

In here, Cw is water content of the sample (wt%), ΔH_0 stands for the activation enthalpy, and α, β and r stand for empirical power–law constants. By a non–linear global least–squares method, the electrical conductivity of gabbroic melt with different water contents was fitted and the fitted parameter results were listed in Table 4. For the magnitude of water–dependent relation of r (0.43 ± 0.05), it makes clear that the water can dramatically enhance the electrical conductivity of gabbroic melt at conditions of 873–1373 K and 1.0 GPa.

4.3 Comparisons with previous studies

As displayed in Fig. 7, five previously reported results on the electrical

conductivity of natural gabbro samples were employed to compare with our absolutely new results for the electrical conductivity of gabbroic melt (Sato and Ida, 1984; Schilling et al., 1997; Maumus et al., 2005; Dai et al., 2015; Saito and Bagdassarov, 2018). As a whole, our acquired electrical conductivity results on gabbroic melts are obviously higher than those of natural gabbro at temperature range of 873–1373 K and pressure of 1.0 GPa. Both Sato and Ida (1984) and Schilling et al. (1997) have already performed the electrical conductivity measurements on natural gabbro at high temperature and atmospheric pressure. In case of the occurrence of temperature–induced partial melting, the electrical conductivity of sample will be increased rapidly by several orders of magnitude. However, we find that there is no any relevant information on the water content for their previously reported electrical conductivity results on those of listed melting–bearing natural gabbro samples. The electrical conductivity results of natural gabbro containing 34 vol% melt from Maumus et al. (2005) are much lower than those of our present gabbroic melt, and the obvious discrepancy is possibly caused from the differentiation of the chemical composition and water content of gabbroic melt. In comparison with Saito and Bagdassarov (2018), there is a jump of three orders of magnitude in the electrical conductivity of sample, which is possibly originated from a relatively larger influence of melt volume percentage. As far as the previously reported electrical conductivity of natural gabbro with a relatively lower water content of ~610 ppm and free of any melt by Dai et al. (2015) at pressures of 0.5–2.0 GPa, there is an approximate electrical conductivity result on the anhydrous gabbroic melt to be observed in the present

studies. And however, the dependence of electrical conductivity of anhydrous and hydrous gabbroic melts on the temperature, pressure and water content is still scarce under high–temperature and high–pressure conditions until now.

It is well known that the gabbroic melt is belonging to one type of representative calc–alkaline igneous rock. As usual, previously available conductivity results confirmed that the electrical conductivity of calc–alkaline igneous rock melts (i.e. dacitic melt, andesitic melt and basaltic melt) is also highly sensitive to the influential factor of the degree of depolymerization at high temperature and high pressure (Ni et al., 2011; Laumonier et al., 2015; Guo et al., 2017). The degree of depolymerization can be characterized by the ratio of non–bridging oxygen ions per tetrahedrally coordinated cation (NBO/T). As pointed out by Mysen et al. (1982), the magnitude of degree of depolymerization on gabbroic melt can be worked out by our above–mentioned EPMA results in Table 1. And the dependence relation of electrical conductivity of gabbroic melts and degree of depolymerization was clearly displayed in Fig. 8 under conditions of four different water contents (i.e. 0, 2.59 wt%, 5.92 wt% and 8.32 wt%), 1373 K and 1.0 GPa. Under constant degree of depolymerization, it makes clears that a relatively lower electrical conductivity is observed in the anhydrous gabbroic melt under condition of 1373 K and 1.0 GPa. With the rise of water content, the electrical conductivity of gabbroic melts dramatically increases, whereas the variation degree for the electrical conductivity gradually reduces. At the same time, we also compared the presently obtained electrical conductivity results for anhydrous and hydrous gabbroic melts with other three representative calc–alkaline

igneous melts reported by Ni et al. (2011), Laumonier et al. (2015) and Guo et al. (2017), as detailedly illustrated in Fig. 8. On the base of the previously calculating method for the degree of depolymerization (NBO/T) of melt transforming the detailed EPMA data, the magnitudes in the degree of depolymerization for our present gabbroic melt and other three representative calc–alkaline igneous rock melts (i.e. dacitic melt, andesitic melt and basaltic melt) are 0.65, 0.07, 0.35 and 0.81, respectively. As a whole, the electrical conductivity of four typical calc–alkaline igneous rock melts will increase with the rise of the degree of depolymerization at a fixed water content. As the water content will be enhanced from 0 to 8.32 wt%, the electrical conductivity of each calc–alkaline igneous rock melts will dramatically increase. It is obviously observed that the correspondent variations in the electrical conductivity of calc–alkaline igneous rock melts along the orders from dacitic melt to andesitic melt to gabbroic melt to basaltic melt tend to gradually reduce, and become more and more convergent, accordingly. To my best knowledge, the magnitude in the degree of depolymerization (NBO/T) for the melt sample is highly positive relation with the content variations of alkali–bearing and alkali earth–bearing cations (i.e. Na^{+}, K^{+}, Ca^{2+}, Mg^{2+}, etc.) (Mysen et al., 1982; Lee et al., 2003; Di Genova et al., 2015). Just as presented the EPMA results, the total contents of alkali cations and alkali–earth cations are determined as the 11.54 wt% of dacitic melt reported by Laumonier et al. (2015), the 20.41 wt% of andesitic melt reported by Guo et al. (2017), the 30.23 wt% of basaltic melt reported by Ni et al. (2011), and as well as the 25.53 wt% of gabbroic melt in this study. And thus, the degree of depolymerization for the calc–

alkaline igneous rock melts along the orders from dacitic melt to andesitic melt to gabbroic melt to basaltic melt will gradually increase, accordingly. On the other hand, previous electrical conductivity results have confirmed that the main charge carriers of the calc–alkaline igneous melts are alkali cations and alkali–earth cations at high temperature and high pressure (Ni et al., 2011; Laumonier et al., 2015; Guo et al., 2017; Chen et al., 2018). And thus, the influence of the degree of depolymerization on the electrical conductivity of melt is possibly caused from the concentration of the alkali cations and alkali–earth cations. Accordingly, the electrical conductivity of calc–alkaline igneous melts will gradually increase with the rise of alkali cations and alkali–earth cations along the orders from dacitic melt to andesitic melt to gabbroic melt to basaltic melt. In sum, as followed the orders from dacitic melt to andesitic melt to gabbroic melt to basaltic melt, it is very reasonable that the electrical conductivity of calc–alkaline igneous melts will be gradually enhanced with the rise of degree of depolymerization (NBO/T) under conditions of 1373 K and 1.0 GPa.

5 Geophysical implications

As a typical active plate geotectonic boundary, previously available magnetotelluric results have already revealed that the phenomenon of high conductivity anomalies is widespread distributed in the region of mid–ocean ridge (Key et al., 2013; Miensopust et al., 2014). For the representative Mohns ridge of the Arctic Ocean, there widely exist a large number of high conductive layers with their conductivity magnitude within the range of ~0.08–0.32 S m^{-1} at the correspondent depths from 4 km to 7 km (Johansen et al., 2019). All of these acquired seismic and

393 gravitational survey datasets have confirmed that various volume percentages of
394 gabbroic melt widely outcropped in the Mohns ridge of the Arctic Ocean at the depths
395 of ~4–11 km (Géli et al., 1994; Conley and Dunn, 2011). And therefore, the high
396 conductivity anomalies in the Mohns ridge of the Arctic Ocean are possibly correlated
397 with the gabbroic melt at high temperature and high pressure. In conjunction with our
398 presently obtained experimental results on the electrical conductivity of anhydrous
399 and hydrous gabbroic melts at conditions of 873–1373 K and 1.0–3.0 GPa, the typical
400 Hashin–Shtrikman upper bound model and previously available magnetotelluric
401 results, the electrical conductivity of gabbroic melt–olivine system was constructed in
402 detail, as displayed in Fig. 9. All of these influential ingredients including water
403 content and volume percentage were comprehensively considered. During the process
404 of the expansion of mid–ocean ridge caused by the rapid upwelling of asthenosphere
405 mantle, the geothermal distribution exhibited an abnormal behavior in the Mohns
406 ridge of the Arctic Ocean. As pointed out by Johansen et al. (2019), the temperature
407 on the top gabbro layer is approximate to 1373 K along the ultraslow–spreading
408 Arctic mid–ocean Mohns ridge region. In addition, the effect of pressure on the
409 electrical conductivity of gabbroic melt is rather feeble, and it can be neglected.

410 For the representative Mohns ridge of the Arctic Ocean, previously available
411 petrological and geochemical results have already revealed that the range of water
412 content for the crustal rock and melt in the Mohns ridge is ~0.25–2.64 wt% (Neumann
413 and Schilling, 1984; Poreda et al., 1986). The electrical conductivity results of
414 gabbroic melt with two different water contents (anhydrous and a water content of

2.59 wt%) are selected from our present studies. The electrical conductivity of olivine at 1373 K and 1.0 GPa is properly extrapolated from the available experimental data of polycrystalline olivine under conditions of 160 ppm wt water content, 873–1273 K and 4.0–10.0 GPa reported by Dai and Karato (2014). On the variation of volume percentage for the gabbroic melt, the electrical conductivity of a gabbroic melt–olivine system (σ_{HS+}) can be expressed as (Hashin and Shtrikman, 1962),

$$\sigma_{HS+} = \sigma_{melt} + [(1-X_{melt})\cdot[(\sigma_{olivine}-\sigma_{melt})^{-1} + X_{melt}/(3\cdot\sigma_{melt})]^{-1} \quad (7)$$

In here, the signals of σ_{melt} and $\sigma_{olivine}$ stand for the electrical conductivity of gabbroic melt from the present study and that of polycrystalline olivine with a certain water content of 160 ppm wt from Dai and Karato (2014), respectively; X_{melt} stands for the volume percentage of gabbroic melt.

The electrical conductivity of gabbroic melt–olivine system with different volume percentage of gabbroic melt was successfully worked out at 1373 K and 1.0 GPa, as displayed in Fig. 9. For the gabbroic melt–olivine system with a certain volume percentage of gabbroic melt, the electrical conductivity increases with the rise of water content in gabbroic melt. As far as the gabbroic melt containing a fixed water content, the electrical conductivity of gabbroic melt–olivine system gradually enhances as the volume percentage of gabbroic melt increases. As pointed out by Johansen et al. (2019), the range of electrical conductivity for the HCL in the Mohns ridge is ~0.08–0.32 S m^{-1}, as displayed in the orange region of Fig. 9. For the anhydrous gabbroic melt, the required volume percentage for the high conductivity anomalies the ultraslow-spreading Arctic mid-ocean Mohns ridge region falls within

the range of ~2.93–34.69 vol%, which is in good agreement with previously inferred results from geophysical observations (Géli et al., 1994; Conley and Dunn, 2011). When the water content of gabbroic melt increases, the required volume percentage for the HCL reduces accordingly. As for the gabbroic melt with a relatively high water content of 2.59 wt%, its volume percentage range of ~2.63–23.63 vol% is enough to explain the high conductivity anomalies. In summary, the high conductivity anomalies in the Mohns ridge of the Arctic Ocean could be interpreted by the anhydrous and hydrous gabbroic melt, and our present electrical conductivity results for gabbroic melt with different water contents can provide an important constraint for the water content and volume percentage of gabbroic melt at depth range of ~4–7 km within the Mohns ridge region of the Arctic Ocean.

Conclusions

In the present studies, the electrical conductivity of gabbroic melt with different water contents of 0–8.32 wt% were measured at temperatures of 873–1373 K and pressures of 1.0–3.0 GPa. For the gabbroic melt with a fixed water content of 2.59 wt%, the electrical conductivity of the sample decreases slightly with the rise of pressure, and its corresponding activation energy and activation volume are determined as 0.87 ± 0.04 eV and –1.98 ± 0.02 cm^3 $mole^{-1}$, respectively. When water content of gabbroic melt enhances from 0 to 8.32 wt% under the certain conditions of 873–1373 K and 1.0 GPa, the electrical conductivity of gabbroic melts tends to visibly increase, and whereas the activation enthalpy gradually reduces from 0.93 eV to 0.63

eV, accordingly. Furthermore, the functional relation models for the electrical conductivity of gabbroic melt with the variations of temperature, pressure and water content are constructed at high–temperature and high–pressure conditions, respectively. By virtue of typical Hashin–Shtrikman upper bound model, the electrical conductivity of gabbroic melt–olivine system on the variation of melt volume percentage is calculated under the conditions of four different water contents of gabbroic melt (i.e. 0, 2.59 wt%, 5.92 wt% and 8.32 wt%), 1373 K and 1.0 GPa, which can be employed to reasonably explain the high conductivity anomalies in the Mohns ridge of the Arctic Ocean observed by the previously available field MT results.

Data availability. The data that support the findings of this study are available from the first author upon reasonable request.

Acknowledgements. We thank the editor of Professor Yang Chu from Institute of Geology and Geophysics, Chinese Academy of Sciences, and two anonymous reviewers for their very constructive and enlightened comments and suggestions in the reviewing process, which helped us greatly in improving the manuscript. This research was financially supported by the NSF of China (grant number 42072055 and 42274137) and the Youth Innovation Promotion Association of CAS (grant number 2019390).

Declaration of competing interest. The authors declare that they have no conflict of interest.

References

Almeev, R., Holtz, F., Koepke, J., Haase, K., and Devey, C.: Depths of partial crystallization of H_2O-bearing MORB: Phase equilibria simulations of basalts at the MAR near Ascension Island (7–11°S), J. Petrol., 49, 25–45, 2008.

Chen, J. Y., Gaillard, F., Villaros, A., Yang, X. S., Laumonier, M., Jolivet, L., Unsworth, M., Hashim, L., Scaillet, B., and Richard, G.: Melting conditions in the modern Tibetan crust since the Miocene, Nat. Commun., 9, 3515, https://doi.org/10.1038/s41467-018-05934-7, 2018.

Conley, M. M. and Dunn, R. A.: Seismic shear wave structure of the uppermost mantle beneath the Mohns Ridge, Geochem. Geophys. Geosyst., 12, Q0AK01, https://doi.org/10.1029/2011GC003792, 2011.

Dai, L. D., Li, H. P., Hu, H. Y., and Shan, S. M.: Experimental study of grain boundary electrical conductivities of dry synthetic peridotite under high-temperature, high-pressure, and different oxygen fugacity conditions, J. Geophys. Res. Solid Earth, 113, B12211, https://doi.org/10.1029/2008JB005820, 2008.

Dai, L. D. and Karato, S. I.: Electrical conductivity of pyrope-rich garnet at high temperature and high pressure, Phys. Earth Planet. Inter., 176, 83–88, 2009a.

Dai, L. D. and Karato, S. I.: Electrical conductivity of orthopyroxene: Implications for the water content of the asthenosphere, Proc. Jpn. Acad. Ser. B, 85, 466–475, 2009b.

Dai, L. D. and Karato, S. I.: Electrical conductivity of wadsleyite at high temperatures

and high pressures, Earth Planet. Sci. Lett., 287, 277–283, 2009c.

Dai, L. D., Li, H. P., Hu, H. Y., Shan, S. M., Jiang, J. J., and Hui, K. S.: The effect of chemical composition and oxygen fugacity on the electrical conductivity of dry and hydrous garnet at high temperatures and pressures, Contrib. Mineral. Petrol., 163, 689–700, 2012.

Dai, L. D., Li, H. P., Hu, H. Y., Jiang, J. J., Hui, K. S., and Shan, S. M.: Electrical conductivity of $Alm_{82}Py_{15}Grs_3$ almandine-rich garnet determined by impedance spectroscopy at high temperatures and high pressures, Tectonophysics, 608, 1086–1093, 2013.

Dai, L. D., Hu, H. Y., Li, H. P., Jiang, J. J., and Hui, K. S.: Effects of temperature, pressure and chemical composition on the electrical conductivity of granite and its geophysical implications, Am. Mineral., 99, 1420–1428, 2014.

Dai, L. D. and Karato, S. I.: The effect of pressure on the electrical conductivity of olivine under the hydrogen-rich conditions, Phys. Earth Planet. Inter., 232, 51–56, 2014.

Dai, L. D., Hu, H. Y., Li, H. P., Hui, K. S., Jiang, J. J., Li, J., and Sun, W. Q.: Electrical conductivity of gabbro: The effects of temperature, pressure and oxygen fugacity, Eur. J. Mineral., 27, 215–224, 2015.

Dai, L. D., Hu, H. Y., Li, H. P., Wu, L., Hui, K. S., Jiang J. J., and Sun, W. Q.: Influence of temperature, pressure, and oxygen fugacity on the electrical conductivity of dry eclogite, and geophysical implications, Geochem. Geophys. Geosyst., 17, 2394–2407, 2016.

Dai, L. D. and Karato, S. I.: Electrical conductivity of Ti–bearing hydrous olivine aggregates at high temperature and high pressure, J. Geophys. Res. Solid Earth, 125, e2020JB020309, https://doi.org/10.1029/2020JB020309, 2020.

Di Genova, D., Morgavi, D., Hess, K. U., Neuville, D. R., Borovkov, N., Perugini, D., and Dingwell, D. B.: Approximate chemical analysis of volcanic glasses using Raman spectroscopy, J. Raman Spectrosc., 46, 1235–1244, 2015.

Dixon, J. B., Stolper, E. M., and Holloway, J. R.: An experimental study of water and carbon dioxide solubilities in mid-ocean ridge basaltic liquids. Part I: Calibration and solubility models, J. Petrol., 36, 1607–1631, 1995.

Förster, M. W. and Selway, K.: Melting of subducted sediments reconciles geophysical images of subduction zones, Nat. Commun., 12, 1320, https://doi.org/10.1038/s41467-021-21657-8, 2021.

Géli, L., Renard, V., and Rommevaux, C.: Ocean crust formation processes at very slow spreading centers: A model for the Mohns Ridge, near 72°N, based on magnetic, gravity, and seismic data, J. Geophys. Res. Solid Earth, 99, 2995–3013, 1994.

Guo, X., Li, B., Ni, H. W., and Mao, Z.: Electrical conductivity of hydrous andesitic melts pertinent to subduction zones, J. Geophys. Res. Solid Earth, 122, 1777–1788, 2017.

Hashin, Z. and Shtrikman, S.: A variation approach to the theory of effective magnetic permeability of multiphase materials, J. Appl. Phys., 33, 3125–3131, 1962.

Hong, M. L., Dai, L. D., Hu, H. Y., Yang, L. F. and Zhang, X. Y.: Pressure-induced

structural phase transitions in natural kaolinite investigated by Raman spectroscopy and electrical conductivity, Am. Mineral., 107, 385–394, 2022.

Hu, H. Y., Dai, L. D., Sun, W. Q., Wang, M. Q., and Jing, C. X.: Constraints on fluids in the continental crust from laboratory-based electrical conductivity measurements of plagioclase, Gondwana Res., 107, 1–12, 2022a.

Hu, H. Y., Jing, C. X., Dai, L. D., Yin, C. Y. and Chen, D. M.: Electrical conductivity of siderite and its implication for high conductivity anomaly in the slab-mantle wedge interface, Front. Earth Sci., 10, 985740, https://doi.org/10.3389/feart.2022.985740, 2022b.

Johansen, S. E., Panzner, M., Mittet, R., Amundsen, H. E. F., Lim, I., Vik, E., Landrø, M., and Arntsen, B.: Deep electrical imaging of the ultraslow-spreading Mohns ridge, Nature, 567, 379–383, 2019.

Key, K., Constable, S., Liu, L. J., and Pommier, A.: Electrical image of passive mantle upwelling beneath the northern East Pacific Rise, Nature, 495, 499–502, 2013.

Laumonier, M., Gaillard, F., and Sifre, D.: The effect of pressure and water concentration on the electrical conductivity of dacitic melts: Implication for magnetotelluric imaging in subduction areas, Chem. Geol., 418, 66–76, 2015.

Lee, S. K., Mysen, B. O., and Cody, G. D.: Chemical order in mixed-cation silicate glasses and melts, Phys. Rev. B, 68, 214206, https://doi.org/10.1103/PhysRevB.68.214206, 2003.

Leuthold, J., Lissenberg, C. J., O'Driscoll, B., Karakas, O., Falloon, T., Klimentyeva, D. N., and Ulmer, P.: Partial melting of lower oceanic crust gabbro: Constraints

566 from poikilitic clinopyroxene primocrysts, Front. Earth Sci., 6, 15,
567 https://doi.org/10.3389/feart.2018.00015, 2018.
568 Li, G. H., Gao, Y., Zhou, Y. Z., Ju, C. H., Shi, Y. T., and Cui, Q. H.: A low-velocity
569 layer atop the mantle transition zone beneath the western Central Asian Orogenic
570 Belt: Upper mantle melting induced by ancient slab subduction, Earth Planet. Sci.
571 Lett., 578, 117287, https://doi.org/10.1016/j.epsl.2021.117287, 2022.
572 Luhr, J. F.: Glass inclusions and melt volatile contents at Parícutin Volcano, Mexico,
573 Contrib. Mineral. Petrol., 142, 261–283, 2001.
574 Maumus, J., Bagdassarov, N., and Schmeling, H.: Electrical conductivity and partial
575 melting of mafic rocks under pressure, Geochim. Cosmochim. Ac., 69, 4703–
576 4718, 2005.
577 Miensopust, M. P., Jones, A. G., Hersir, G. P., and Vilhjálmsson, A. M.: The
578 Eyjafjallajökull volcanic system, Iceland: Insights from electromagnetic
579 measurements, Geophys. J. Int., 199, 1187–1204, 2014.
580 Mysen, B. O., Virgo, D., and Seifert, F. A.: The structure of silicate melts:
581 Implications for chemical and physical properties of natural magma, Rev.
582 Geophys., 20, 353–383, 1982.
583 Neumann, E. R. and Schilling, J. G.: Petrology of basalts from the Mohns–Knipovich
584 Ridge; the Norwegian–Greenland Sea, Contrib. Mineral. Petrol., 85, 209–223,
585 1984.
586 Ni, H. W., Keppler, H., and Behrens, H.: Electrical conductivity of hydrous basaltic
587 melts: Implications for partial melting in the upper mantle, Contrib. Mineral.

588 Petrol., 162, 637–650, 2011.
589 Poreda, R., Schilling, J. G., and Craig, H.: Helium and hydrogen isotopes in ocean–
590 ridge basalts north and south of Iceland, Earth Planet. Sci. Lett., 78, 1–17, 1986.
591 Saito, S. and Bagdassarov, N. S: Laboratory measurements of electrical conductivity
592 in a gabbro of the Oman ophiolite at high–pressures and high–temperatures:
593 Implications for interpretation of resistivity structures of lower oceanic crust, J.
594 Mineral. Petrol. Sci., 113, 112–117, 2018.
595 Sato, H. and Ida, Y.: Low frequency electrical impedance of partially molten gabbro:
596 the effect of melt geometry on electrical properties, Tectonophysics, 107, 105–
597 134, 1984.
598 Schilling, F. R., Partzsch, G. M., Brasse, H., and Schwarz, G.: Partial melting below
599 the magmatic arc in the central Andes deduced from geoelectromagnetic field
600 experiments and laboratory data, Phys. Earth Planet. Inter., 103, 17–31, 1997.
601 Shaw, A. M., Behn, M. D., Humphris, S. E., Sohn, R. A., and Gregg, P. M.: Deep
602 pooling of low degree melts and volatile fluxes at the 85°E segment of the
603 Gakkel Ridge: Evidence from olivine-hosted melt inclusions and glasses, Earth
604 Planet. Sci. Lett., 289, 311–322, 2010.
605 Shen, Y. and Forsyth, D. W.: Geochemical constraints on initial and final depths of
606 melting beneath mid-ocean ridges, J. Geophys. Res. Solid Earth, 100, 2211–2237,
607 1995.
608 Sim, S. J., Spiegelman, M., Stegman, D. R., and Wilson, C.: The influence of
609 spreading rate and permeability on melt focusing beneath mid-ocean ridges, Phys.

610 Earth Planet. Inter., 304, 106486, https://doi.org/10.1016/j.pepi.2020.106486,
611 2020.
612 Stolper, E.: The speciation of water in silicate melts, Geochim. Cosmochim. Ac., 46,
613 2609–2620, 1982.
614 Turner, S. J. and Langmuir, C. H.: Sediment and ocean crust both melt at subduction
615 zones, Earth Planet. Sci. Lett., 584, 117424,
616 https://doi.org/10.1016/j.epsl.2022.117424, 2022.
617 Tyburczy, J. A. and Roberts, J. J.: Low frequency electrical response of polycrystalline
618 olivine compacts: Grain boundary transport, Geophys. Res. Lett., 17, 1985–1988,
619 1990.
620 Wallace, P. J.: Volatiles in subduction zone magmas: concentrations and fluxes based
621 on melt inclusion and volcanic gas data, J. Volcanol. Geoth. Res., 140, 217–240,
622 2005.
623 White, R. S., Minshull, T.A., Bickle, M. J., and Robinson, C. J.: Melt generation at
624 very slow-spreading oceanic ridges: Constraints from geochemical and
625 geophysical data, J. Petrol., 42, 1171–1196, 2001.
626 Wu, K., Ling, M. X., Hu, Y. B., Guo, J., Jiang, X. Y., Sun, S. J., Liang, H. Y., Liu, X.,
627 and Sun, W. D.: Melt-fluxed melting of the heterogeneously mixed lower arc
628 crust: A case study from the Qinling orogenic belt, Central China, Geochem.
629 Geophys. Geosyst., 19, 1767–1788, 2018.

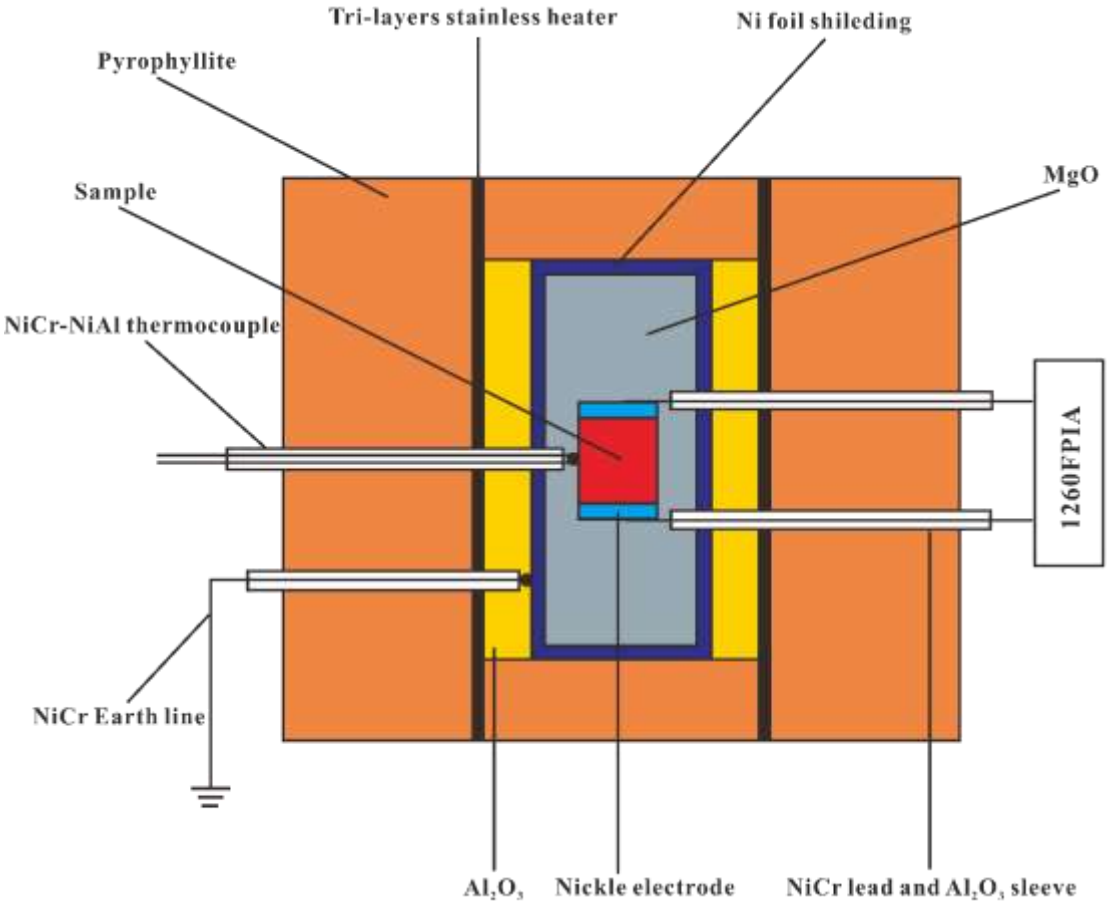

630

631 **Figure 1.** The experimental setup for the electrical conductivity measurements of
632 gabbroic melt at high temperatures and high pressures.

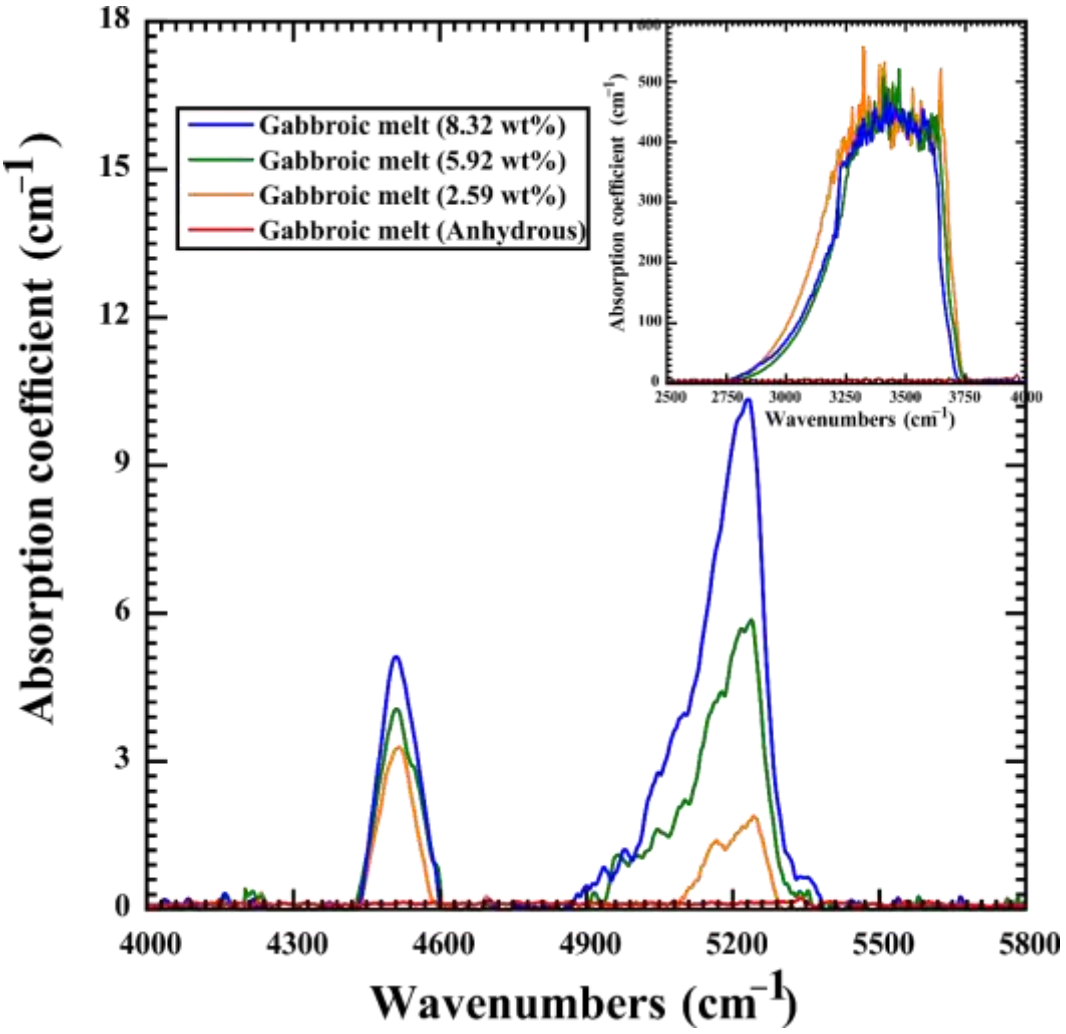

633

634 **Figure 2.** The representative FT–IR spectra of the gabbroic melt with various water
635 contents in the wavenumbers range of 4000–5800 cm^{-1} and 2500–4000 cm^{-1}.

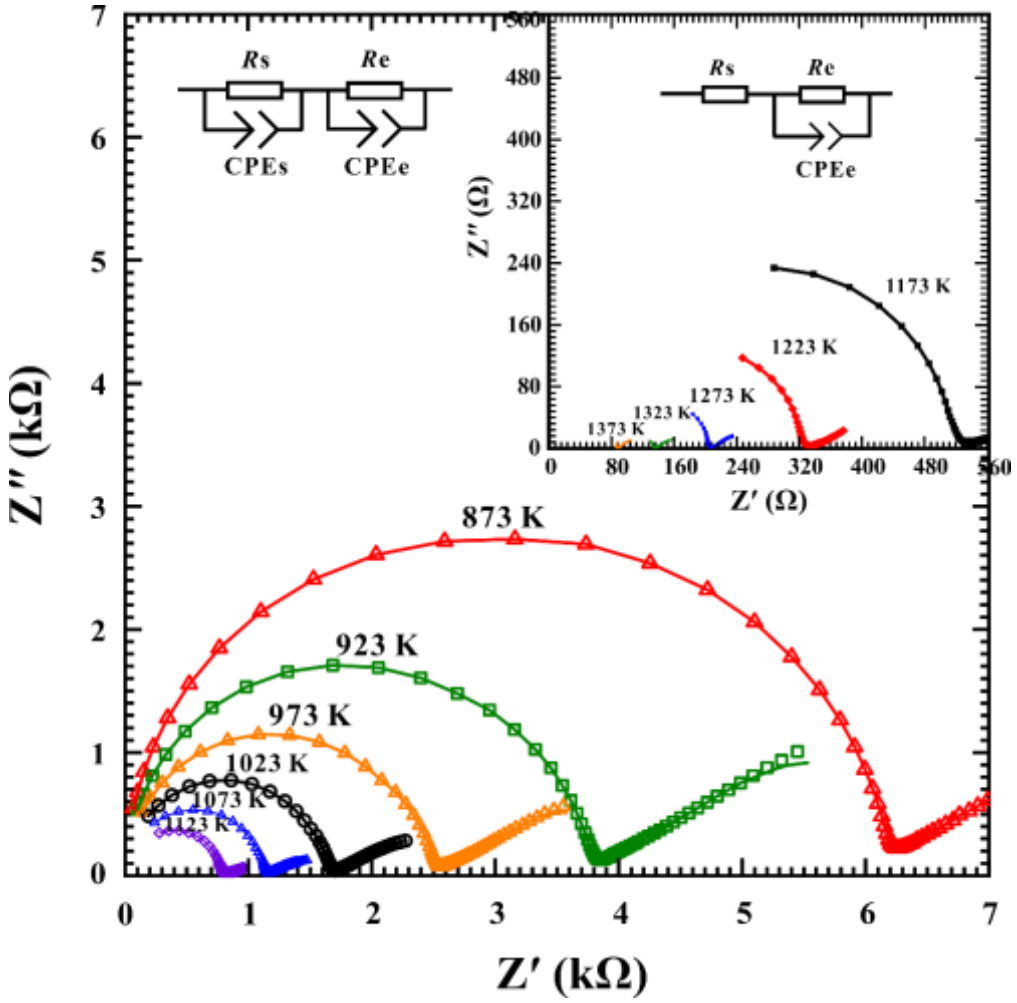

636

637 **Figure 3.** Typical complex impedance spectra for gabbroic melt with a fixed water
638 content of 2.59 wt% at temperatures of 873–1373 K and pressure of 2.0 GPa in the
639 frequency range from 10^0 Hz to 10^6 Hz. The fitting results for the experimental data
640 are displayed by using the solid line.

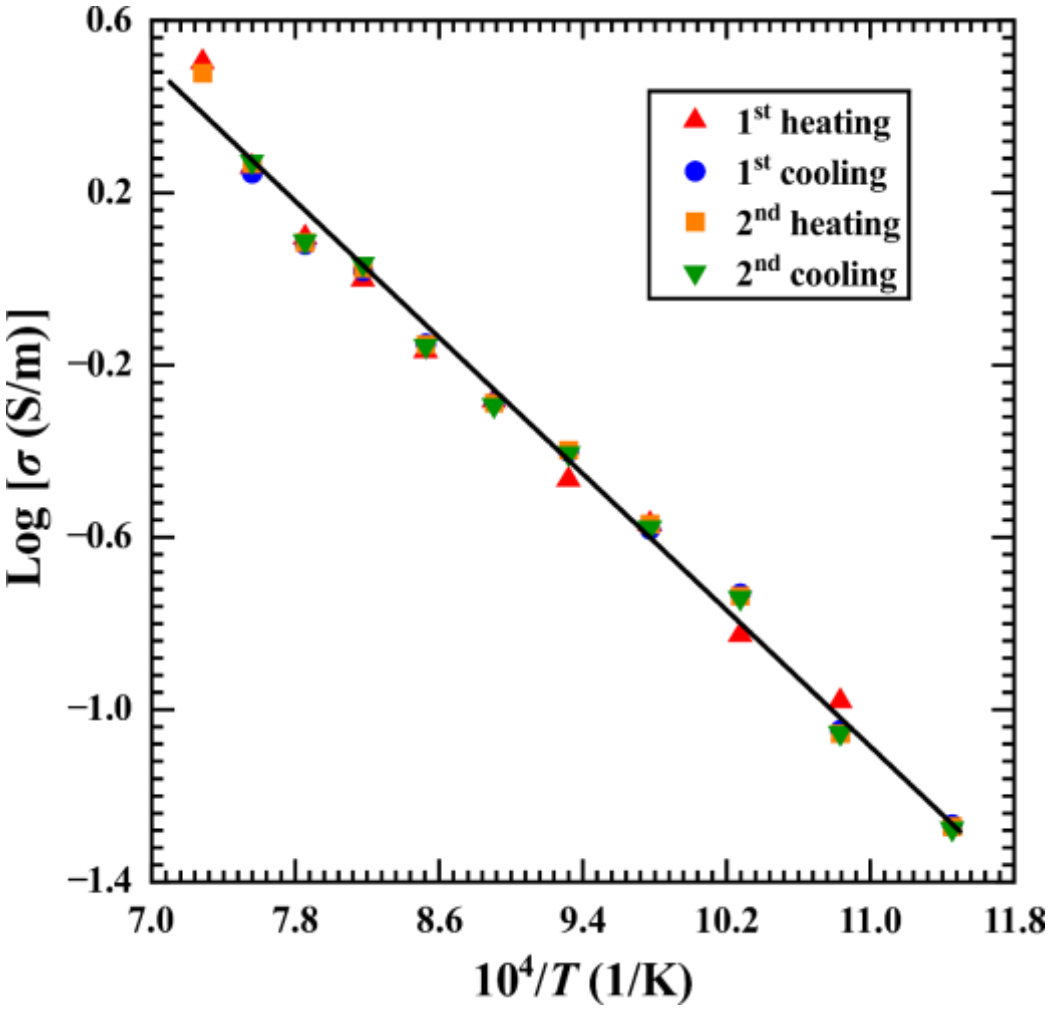

641

642 **Figure 4.** The electrical conductivity of gabbroic melt with a fixed water content of
643 2.59 wt% among two heating–cooling cycles at a pressure of 3.0 GPa.

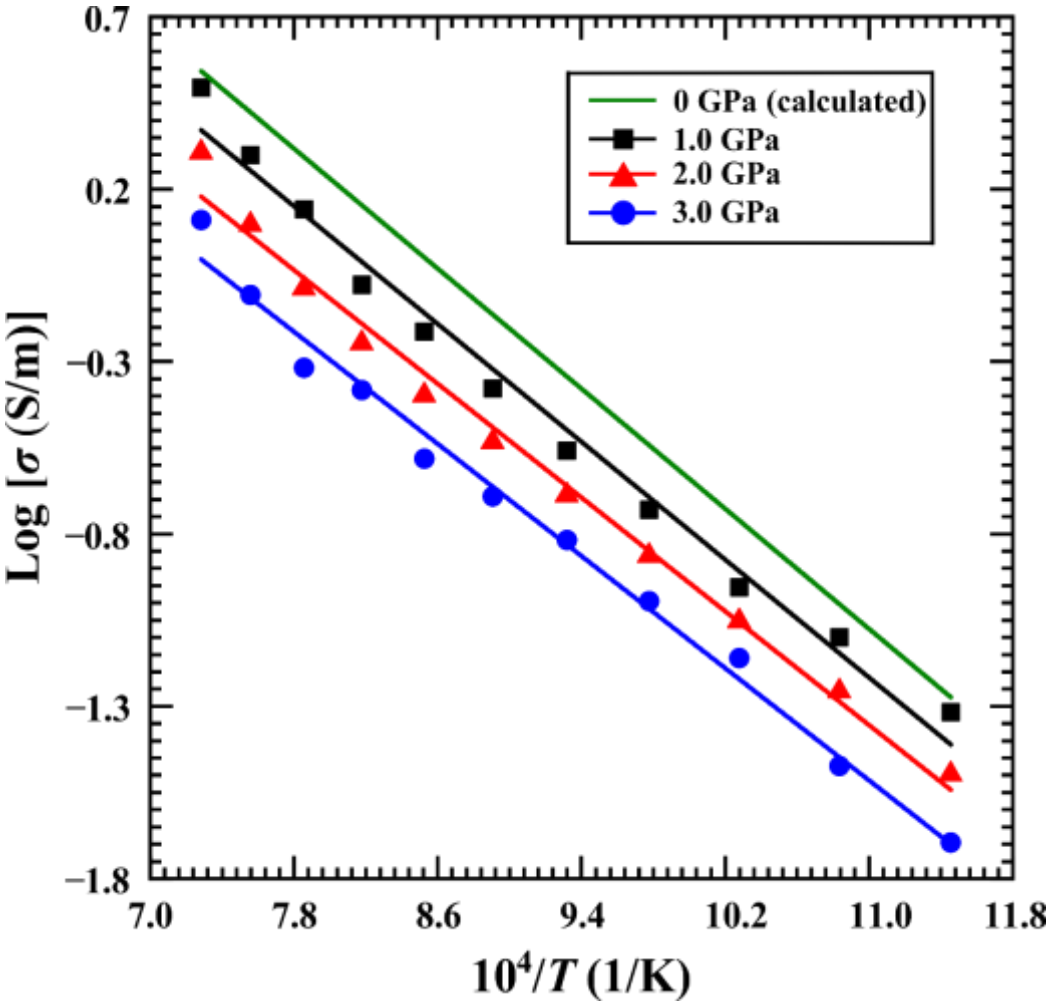

644

645 **Figure 5.** Influence of pressure on the electrical conductivity of gabbroic melt with a
646 fixed water content of 2.59 wt% at the temperature ranges of 873–1373 K.

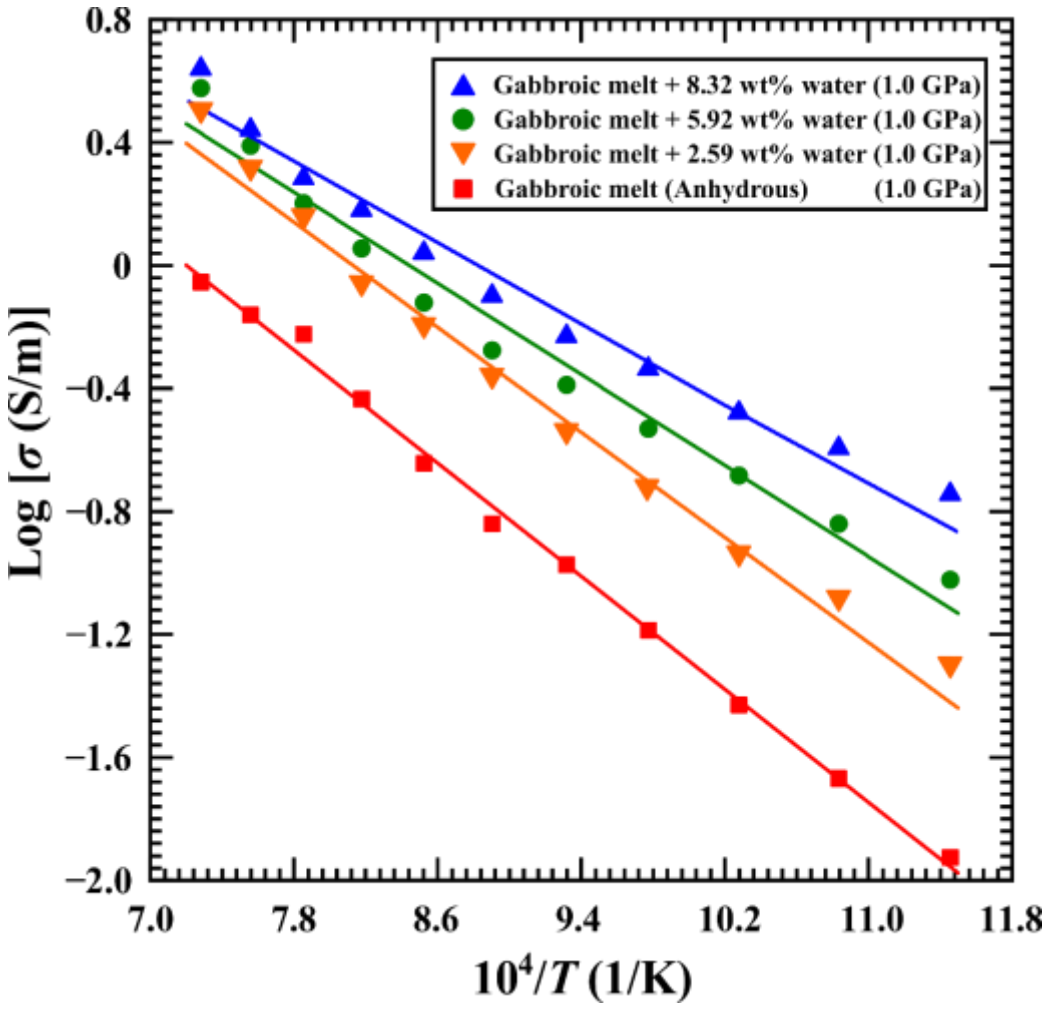

Figure 6. Logarithmic electrical conductivity of gabbroic melts with four different water contents as a function of reciprocal temperature at conditions of 873–1373 K and 1.0 GPa.

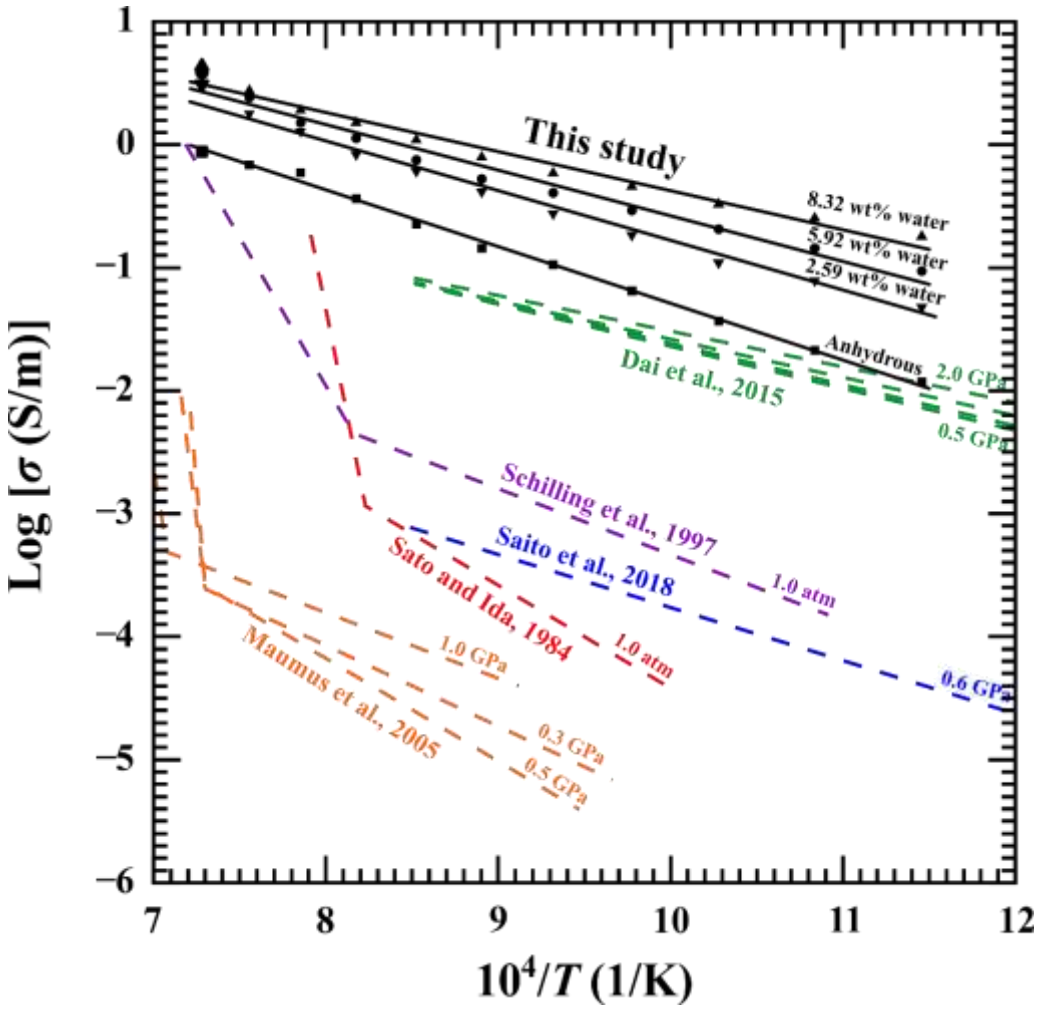

651

652 **Figure 7.** Comparison of electrical conductivity of gabbroic melts with the previously
653 reported results from five natural gabbro samples at high–temperature and high–
654 pressure conditions.

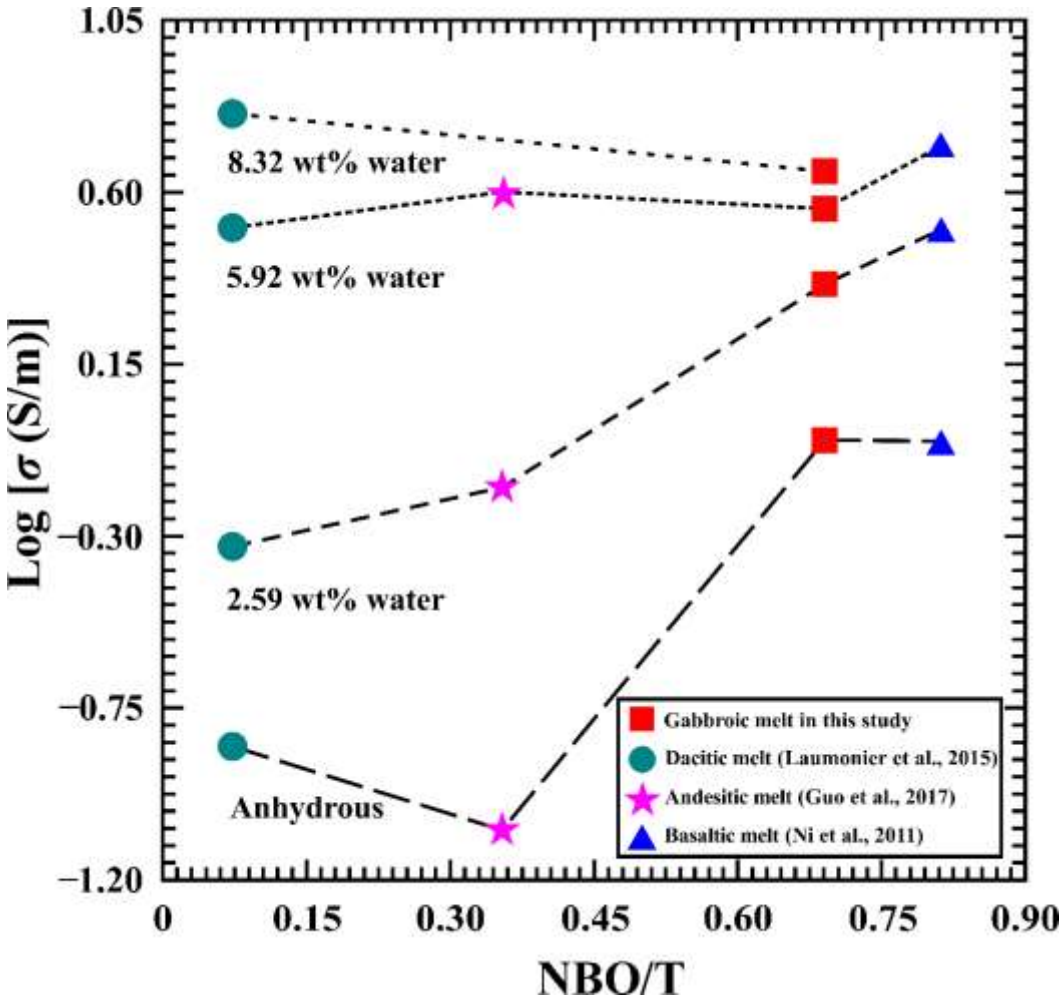

655

656 **Figure 8.** Variation of electrical conductivity of gabbroic melt and three
657 representative calc–alkaline igneous rock melts with the degree of depolymerization
658 (NBO/T) under conditions of four different water contents (i.e. 0, 2.59 wt%, 5.92 wt%
659 and 8.32 wt%), 1373 K and 1.0 GPa. Data source: basaltic melt from Ni et al. (2011),
660 andesitic melt from Guo et al. (2017), and dacitic melt from Laumonier et al. (2015).

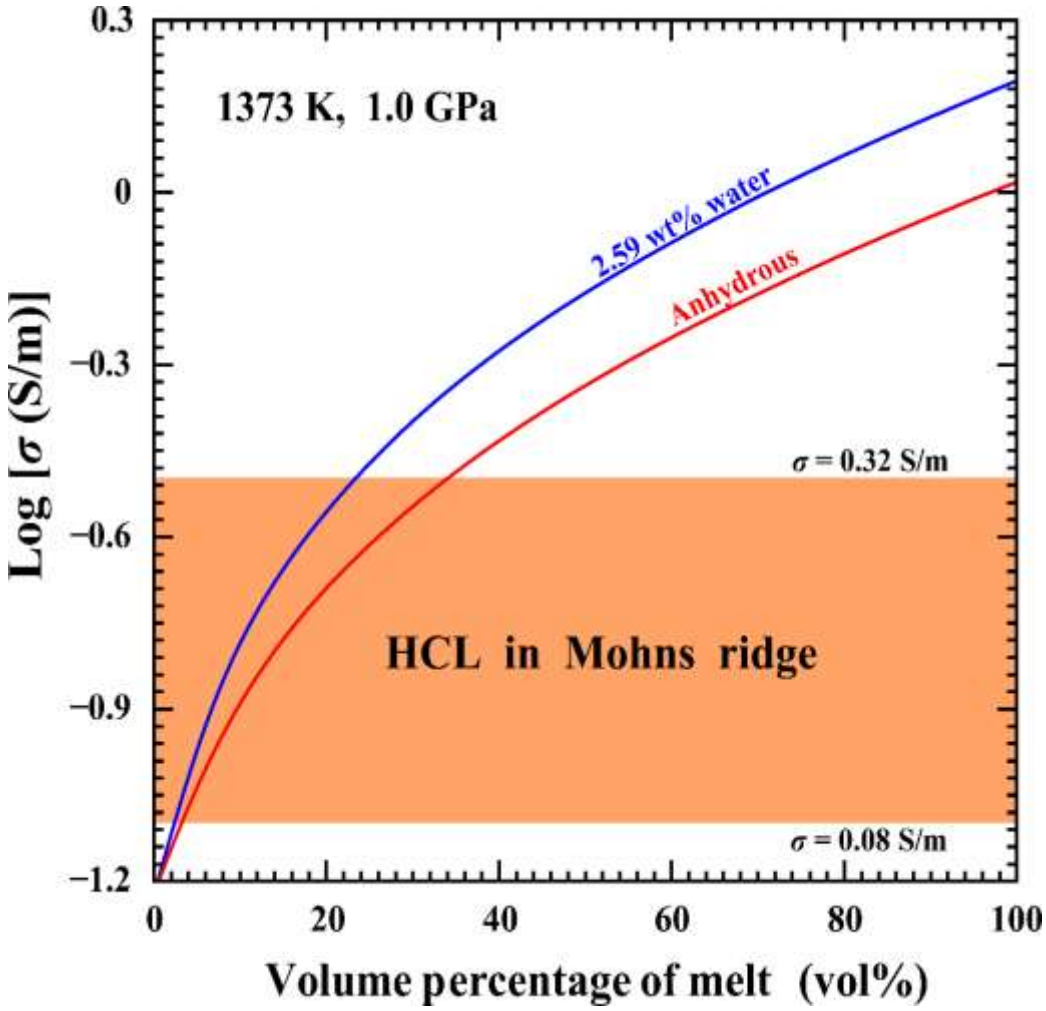

661

662 **Figure 9.** The electrical conductivity for the gabbroic melt–olivine system at
663 temperature of 1373 K and 1.0 GPa, calculated with Eq. 7 of the Hashin–
664 Shtrikman upper bound model. The electrical conductivity of olivine from Dai
665 and Karato (2014) was adopted as $\sigma_{olivine}$. The orange region indicates the gabbro
666 layer within the electrical conductivity range of 0.08–0.32 S m^{-1} along the
667 ultraslow–spreading Arctic mid–ocean Mohns ridge region (Johansen et al.,
668 2019).

669 **Table 1.** The chemical composition of the gabbroic melts by virtue of the electronic
670 probe microscopy analysis (EPMA).

Sample	SiO_2	TiO_2	Al_2O_3	FeO	MnO	MgO	CaO	Na_2O	K_2O	Total (wt%)
Gabbroic melt (anhydrous)	51.32	0.56	12.37	9.93	0.20	11.06	11.82	2.15	0.50	99.91
Gabbroic melt (2.59 wt% water)	51.22	0.55	12.40	9.92	0.18	11.29	11.72	2.19	0.48	99.95
Gabbroic melt (5.92 wt% water)	51.23	0.57	12.40	9.87	0.18	11.28	11.70	2.21	0.47	99.91
Gabbroic melt (8.32 wt% water)	51.22	0.57	12.40	9.88	0.17	11.27	11.69	2.21	0.46	99.86

671

672 **Table 2.** Fitted parameters of Arrhenius relation for the electrical conductivity of
673 hydrous and anhydrous gabbroic melts under conditions of 873–1373 K and 1.0–3.0
674 GPa.

Sample	*T* (K)	*P* (GPa)	Water content Before experiment (wt%)	Water content After experiment (wt%)	Log σ_0 (σ_0 in S m^{-1})	ΔH (eV)
DW201	873–1373	1.0	8.32 ± 0.02	8.30 ± 0.01	2.80 ± 0.16	0.63 ± 0.03
DW204	873–1373	1.0	5.92 ± 0.01	5.90 ± 0.02	3.13 ± 0.18	0.74 ± 0.04
DW208	873–1373	1.0	2.59 ± 0.01	2.57 ± 0.01	3.48 ± 0.15	0.85 ± 0.03
DW209	873–1373	2.0	2.59 ± 0.03	2.58 ± 0.01	3.18 ± 0.13	0.83 ± 0.03
DW212	873–1373	3.0	2.59 ± 0.01	2.50 ± 0.02	2.79 ± 0.11	0.81 ± 0.03
DW210	873–1373	1.0	0	0	3.31 ± 0.08	0.93 ± 0.02

675

676 **Table 3.** Parameter values for the electrical conductivity of gabbroic melt with water
677 content of 2.59 wt% at pressures of 1.0–3.0 GPa. The equation $\sigma = \sigma_0 \cdot \exp(-\frac{\Delta U + P\Delta V}{kT})$
678 is adopted for the globally fitting of electrical conductivity data. In consideration of
679 a strong dependence of the pre–exponential factor (σ_0) on the pressure, we used the
680 relation $\sigma_0 = A_0 \cdot (1 - BP)$.

σ_0 (S m^{-1})	B (GPa^{-1})	ΔU (eV)	ΔV (cm^3 mole^{-1})
A_0 = 2623.27±1.41	B = 0.22±0.03	0.87±0.04	–1.98±0.52

681

682 **Table 4.** Parameter values for the electrical conductivity of gabbroic melts with
683 different water contents under conditions of 873–1373 K and 1.0 GPa. The
684 equation $\sigma = (A_1+A_2\cdot C_w^r)\cdot\exp(\frac{-\Delta H_0-\alpha C_w^\beta}{RT})$ is adopted for the globally fitting of electrical
685 conductivity data.

A_1 (S m^{-1})	A_2 (S m^{-1})	ΔH_0 (eV)	α	β	r
6760±234	66069±240	1.03±0.04	34.85±2.24	17.70±1.31	0.43±0.05

686